# **RESEARCH LETTER**

**Open Access** 

# Nonlinear black-box approaches and data fusion for ocean bathymetry modeling in south Iran

M. A. Mohammad<sup>1</sup>, I. Jazireeyan<sup>1</sup>, M. Pirooznia<sup>2\*</sup> and S. Jin<sup>3,4</sup>

### **Abstract**

The detailed knowledge of bathymetry pattern represents a key factor in the deep understanding of ocean processes, physical oceanography, biology, ecohydraulics, and marine geology. However, the accuracy of bathymetry modeling is still low from satellite altimetry, gravity model, and shipborne gravity data. In this paper, a novel scheme is proposed based on black-box theory for regional bathymetry modeling in the Persian Gulf and the Oman Sea via geodetic data sources such as satellite altimetry, gravity model, and shipborne gravity data. Multi-Layer Perceptron (MLP), Adaptive Neuro-Fuzzy Inference System (ANFIS), and Local Linear Model Tree (LOLIMOT) algorithms are used as nonlinear black-box tools to identify the basic mathematical model. The geoid height, gravity gradient, and gravity anomaly are used as inputs to these artificial intelligence models, with the GEBCO bathymetry model as the output. The derived basic model is further improved by assimilating with the shipborne bathymetry measurements using the 3D variational optimization method to determine the final bathymetry model. The model is validated by the shipborne bathymetry in control tracks of regions Chabahar, Genaveh, and Alamshah, and the results show high accuracy and reliability with root mean square errors (RMSEs) of about 4, 0.8, and 0.92 m, respectively. The proposed approach is valuable for various uses in marine science.

Keywords Bathymetry modeling, Geoid height, Gravity, Black box

# Introduction

Water currents and tides are generally influenced by the overall contours of ocean basins, along with the smaller, prominent ocean ridges and seamounts (Wollheim et al. 2022). Direct measurements of seafloor topography are usually performed using ships fitted with echo sounders, which can deliver highly detailed bathymetric data;

however, the high operational costs render this method economically impractical for extensive coverage (Peng et al. 2022). Thus, nowadays, indirect measurements based on remote sensing techniques have garnered much interest for bathymetry and natural resources monitoring and modeling purposes (Jin et al. 2024; Pirone et al. 2023). It has been established for some time that gravity can be utilized to model the seafloor's shape (Zhu And Wiberg 2022). The seafloor acts as the shallowest density interface within the oceanic environment, and variations in its depth can be viewed as height changes of mass elements, determined by the density contrast between rock and seawater. These depth variations affect the local gravity field. Parker (1973) suggested a strong correlation exists between seafloor topography and sea level gravity anomalies. Alterations in bathymetry lead to gravitational distortions that impact sea surface height, enabling

\*Correspondence:

M. Pirooznia

m\_pirooznia@sbu.ac.ir

<sup>&</sup>lt;sup>4</sup> School of Surveying and Land Information Engineering, Henan Polytechnic University, Jiaozuo 454003, China



 $<sup>^{\</sup>rm 1}$  Faculty of Geodesy and Geomatics Engineering, K. N. Toosi University of Technology, Tehran, Iran

<sup>&</sup>lt;sup>2</sup> Faculty of Civil, Water and Environmental Engineering, Shahid Beheshti University, Tehran, Iran

<sup>&</sup>lt;sup>3</sup> School of Artificial Intelligence, Anhui University, Hefei 230601, China

Mohammad et al. Geoscience Letters (2025) 12:53

the reconstruction of underlying features like seamounts and ridges (Wiehle et al., 2016).

Recent advances have highlighted the importance of improved gravity-based methods for reliable bathymetric prediction (An et al. 2022). The introduction of satellite altimetry has significantly enhanced global marine gravity modeling (Wan et al. 2019; Xu et al. 2023). Successive satellites equipped with altimeters have delivered precise and dense measurements of sea surface height, which can be transformed into estimates of seafloor topography. Lecours et al. (2016) provided a comprehensive literature review of the methods, technologies, and datasets employed in bathymetry modeling.

Recently, machine learning techniques, particularly neural networks, have gained wide application in seafloor modeling. Zhou et al. (2024, 2025) developed global seafloor models using multi-layer perceptrons and multi-source marine geodetic data, demonstrating the capability of neural networks for large-scale bathymetry estimation. Similarly, Zhu and Wiberg (2022) applied MLP in a regional case study of the Caribbean Sea, confirming the potential of neural networks for localized bathymetric modeling. Moreover, deep learning approaches such as convolutional neural networks (CNNs) have shown strong performance in seafloor topography inversion from multi-source gravity data (Ge et al. 2025), while fully connected deep neural networks (FCDNNs) have been applied for seabed depth prediction using multi-scale gravity anomalies, yielding promising results in regional studies (Yuan et al. 2025). These advances highlight the growing role of machine learning in enhancing the resolution and accuracy of bathymetric models, which motivates the methodology adopted in this study.

To address the limitations of traditional physical models, especially the constraints of Parker-based approaches, black-box modeling frameworks rooted in artificial intelligence techniques have been increasingly employed. More specifically, the most widely used physical formulas are based on the well-known Parker (1973) model (Parker 1973; Oldenburg 1974; Watts 1978). The Parker mathematical formula is based on the density difference between sea water and sea floor, mean thickness of the crust, mean depth of sea water, and densities of the Earth's mantle and crust. Some inherent difficulties in applying the Parker model are the lack of enough knowledge for the estimation of model parameters and the linearized approximation in the implementation procedure, resulting in bias and computational errors. The determination of bathymetry from gravity anomaly is essentially an inverse problem, which is regarded as a poorly defined problem that may have multiple unstable solutions, necessitating some form of regularization (Smith And Sandwell, 2005; Dick et al. 2003; Tenzer et al. 2015; Yonkee And Weil 2015; Mitchell et al. 2021). In such a case, the bathymetry outcomes associated with high-frequency components are highly oscillatory, and thus a low-pass filter should be applied to smooth the results (Thompson And Richards 2011; Olive et al. 2015; Abulaitijiang et al. 2019).

In this study, in order to improve the accuracy of bathymetry modeling, the novel scheme based on the black-box theory, which has its roots in the artificial intelligence algorithms, is used to construct the relation between gravity field parameters (geoid height, gravity gradients, gravity anomaly) with bathymetry and to produce a more accurate bathymetry model. Generally, modeling involves abstracting a real process to describe its behavior (Zhang et al. 2022). The goal of scientific modeling is to improve the study of phenomena in order to uncover and understand cause-and-effect relationships, aiming to replicate the 'key characteristics' of the system's behavior by selecting its most significant features (Lei et al. 2023). Thus, modeling techniques can be classified into the following categories (Pirone et al. 2023):

- 1. White-box modeling, in which the model is fully understood and can be developed completely based on existing knowledge and physical intuition (Ma et al. 2022).
- 2. Grey-box modeling, where some physical insight is accessible, but numerous parameters still need to be ascertained from the collected data (Hossain et al. 2021)
- 3. Black-box modeling, which relies merely on the data's behavior (data-driven) without prior knowledge of the system (Zhang et al. 2022). As mentioned by Pirone et al. (2023) among others, the model describes how the output data may be connected to the inputs, not how the system works from physical perspective. Therefore, it describes the system's dynamics (such as delays, speed, oscillations, and more), although interpreting the results physically can be complex.

In addition to the issues with the physical models mentioned above, there are other problems that arise, which include: (i) the nonlinear relationship between gravity field parameters and bathymetry is not well captured by existing modeling approaches, highlighting the need for more advanced techniques. (ii) There is an absence of flexibility and robust modeling methods that can effectively handle the complexity of the gravity field-bathymetry relationship, which is crucial for accurate bathymetry mapping and modeling. (iii) The limitations of current methods in terms of computational efficiency, accuracy,

Mohammad et al. Geoscience Letters (2025) 12:53 Page 3 of 18

and interpretability suggest the need for innovative approaches to improve bathymetry modeling and overcome the existing challenges (Thompson And Richards 2011; Olive et al. 2015).

In this study, to overcome the problems mentioned, it is assumed that the mathematical model between gravity field parameters and bathymetry is unknown. Based on previous studies, we know that the relationship between the parameters of the Earth's gravity field and the bathymetry is a nonlinear relationship (Fan et al. 2021), so nonlinear models of black-box theory have been used. The black-box theory, as it was explained above, seeks to find a relation between two sets of data as input and output parts. Here, our input and output data would be gravity field parameters and available bathymetry data, respectively. The gravity field parameters used in this study include geoid height obtained by satellite altimetry, gravity gradient derived by the XGM2019e gravity model, and gravity anomaly, both computed from satellite altimetry using inverse Stokes formula and directly measured by shipborne. For bathymetry data, we use the global GEBCO model to produce a grid of bathymetry consistent with the spatial distribution of our computed gravity anomaly. Now, with the aid of powerful tools of black-box theory, such as Multi-Layer Perceptron (MLP), Adaptive Neuro-Fuzzy Inference System (ANFIS), and Local Linear Model Tree (LOLIMOT), these two sets of input and output data are connected (Pirone et al. 2023). These approaches have been widely validated in recent research, demonstrating their effectiveness in capturing complex nonlinear relationships in gravity-bathymetry studies (Zhou et al. 2024, 2025; Ge et al. 2025; Yuan et al. 2025). This initial step yields a basic model, which is constructed before assimilating observational data; however, the final model of bathymetry in this research is determined by assimilating in situ shipborne measurements by echo sounder with the basic model using 3D vibrational optimization method (Volpe et al. 2019). Therefore, by employing three black-box modeling techniques and integrating gravity data obtained from multiple sources with bathymetric local observations from echo sounders, this study aims to construct a more accurate and reliable bathymetry model, effectively addressing the limitations of traditional approaches.

# Materials and methods

# **Data description**

The region of study is the Persian Gulf and Oman Sea. Specifically, some areas of the Persian Gulf and Oman Sea are selected for more focus due to the availability of local bathymetry data; these regions are the Genaveh and Alamshah in the Persian Gulf, with the locations of (29.1–29.8°N, 49.7–50.6°E) and (25.9–26.6°N, 52.2–52.8°E),

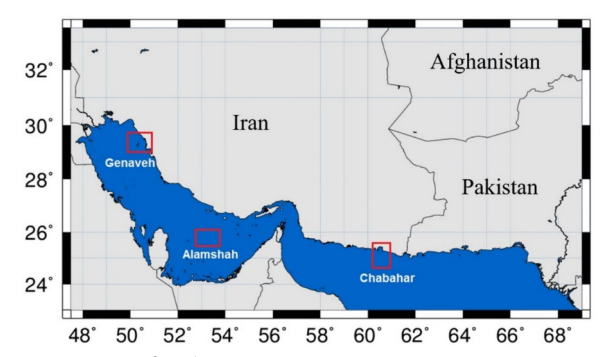


Fig. 1 Region of study

**Table 1** Satellite altimetry features used in this study

Mission	Cycles	Dates
Envisat	008-094	2002-07-22 21:39:36-2010-10-19 02:56:07
Jason-1	001-259	2002-01-15 06:29:49-2009-01-26 08:49:42
Jason-2	001-303	2008-07-12 01:25:39-2016-10-02 11:45:54
Jason-3	001-033	2016-02-17 10:28:53-2017-01-09 15:40:08
Topex	001-365	1992-09-25 05:24:42-2002-08-15 17:44:37
Poseidon	001-361	1992–10-01 16:45:02–2002–07-12 14:28:19
SARAL	001-035	2013-03-15 0:12:50-2016-07-04 11:04:37

respectively, and Chabahar (24.5–25.5°N, 59.4–61.2°E) in the Oman Sea (Fig. 1).

Repeated altimetry measurements at identical locations have been utilized to infer the marine geoid, which is an equipotential surface reflecting the internal mass distribution of the Earth. This surface, influenced by uneven mass, is connected to both the distribution of mass and the external shape (Majumdar And Chander 2011). The external shape relates to topography or bathymetry, while mass distribution is linked to subsurface geological structures. The classical geoid is responsive to mass distribution throughout the Earth. An anomaly (either positive or negative) in the classical geoid may be caused by a bathymetric feature, such as a seamount, trench, or ridge; (ii) a lateral density variation in the lithospheric zone; (iii) an anomaly, deep-seated inside the earth, i.e., below the lithospheric zone, or (iv) any combination of the above three features (Majumdar And Chander 2011). To determine the geoid height using satellite altimetry, the first step is to process altimeter data to determine sea surface height. It is computed from the difference between satellite height and corrected range. In this study, to calculate MSS, the time series of instantaneous sea surface heights (SSH) is first obtained using altimetry data from the satellites listed in Table 1. Then, the least square spectral analysis (LSSA) method is implemented to obtain the tidal components (see (Soltanpour et al. 2017; Pirooznia

Mohammad et al. Geoscience Letters (2025) 12:53 Page 4 of 18

et al. 2016)). By removing the tidal components from SSH time series, the long-term mean sea surface (MSS) is derived. Then the geoid undulation is acquired by subtracting the MSS from the mean dynamic topography (MDT). A global MDT model named MDT-DTU-2012 is used for this purpose. This model has been produced by Danish technical university in 2012 (Knudsen And Andersen 2012). To achieve marine gravity anomaly from satellite altimeters, the computed geoid undulation is converted to along-track geoid gradients, in the north and east directions on a  $1' \times 1'$  grid (deflection components). The inverse Stokes formula (Rummel et al., 1978) is then used to compute marine gravity anomalies from the two gradient components (Smith And Moose 1997). The data sources for this study include (i) Geophysical Data Records (GDR) of satellite altimetry missions shown in Table 1 for estimation of geoid height and gravity anomaly. (ii) As mentioned above, the MDT of DTU for computing geoid height. (iii) The shipborne bathymetry data in Genaveh, Alamshah, and Chabahar regions for the data fusion process. (iv) The XGM2019e gravity model for determination of gravity gradients (Zingerle et al. 2020). In this study, the XGM2019e gravity models up to degree and order 5399 was used to provide gravity data with a spatial resolution of 2 arcminutes. The gravity gradient computations via gravity models is described in Kiamehr and Eshagh (2008) and Petrovskaya and Vershkov (2006). (v) GEBCO global bathymetry data as an output of black-box models. The GEBCO model used in this study is **GEBCO 2019**.

#### **Bathymetry modeling**

The bathymetry modeling process using black-box theory can be outlined as follows:

• Input data:

The input data include gravity field parameters derived by:

- i. Geoid height obtained from satellite altimetry.
- ii. Gravity gradient derived from the XGM2019e gravity model. the gradients are considered along the satellite's flight path (along-track) to accurately capture variations in the geoid or sea surface height along the measurement line.
- iii. Gravity anomaly computed using satellite altimetry (inverse Stokes formula) and shipborne measurements.
- Output data:

The available bathymetry data used as the output data are the global GEBCO model, which provides a grid of bathymetry data consistent with the spatial distribution of the computed gravity anomaly.

- Non-linear black-box models:
  - Powerful black-box techniques, like Multi-Layer Perceptron (MLP), Adaptive Neuro-Fuzzy Inference System (ANFIS), and Local Linear Model Tree (LOLI-MOT), are employed to connect the input gravity field parameters with the output bathymetry data. These black-box models serve as the basic bathymetry models, determining the connection between the earth's gravitational field data and the bathymetry.
- Data assimilation and final bathymetry model:
   The basic bathymetry models are further refined by assimilating in situ shipborne echo sounder measurements. A 3D variational optimization method is used to incorporate the additional bathymetric data and estimate the final bathymetry model.

This integrated approach, leveraging both gravity field data and direct bathymetric measurements, aims to overcome the limitations of relying solely on gravity-based models and improve the overall accuracy and reliability of the bathymetry mapping process. Figure 2 shows the steps of the proposed scheme for bathymetry modeling.

# Non-linear black-box models

In this section, a brief description of nonlinear black-box theory is presented. The aim is to find an appropriate earth gravitational field parameters—bathymetry model based on an error criterion. The system identification problem is defined as follows (Chen et al. 2021):

$$y = G(x, \theta), \tag{1}$$

where x and y are inputs and outputs, respectively, and  $\theta$  is called the parameter of function G. The nonlinear black-box modeling addresses subjects ranging from approximation theory and estimation theory to non-parametric regression, algorithms, and contemporary topics such as neural networks and fuzzy models. It also emphasizes significant connections to traditional statistical techniques in non-parametric regression and density estimation, particularly through kernel methods (Pirone et al. 2023).

In the present case study, Multi-Layer Perceptron (MLP), Adaptive Neuro-Fuzzy Inference System (ANFIS), and Local Linear Model Tree (LOLIMOT) approaches are employed to identify the model function.

#### Multilayer perceptron neural network (MLP)

In recent years, significant efforts have been made to replicate a natural neuron that can capture the features of various phenomena that are also easy to implement Mohammad et al. Geoscience Letters (2025) 12:53 Page 5 of 18

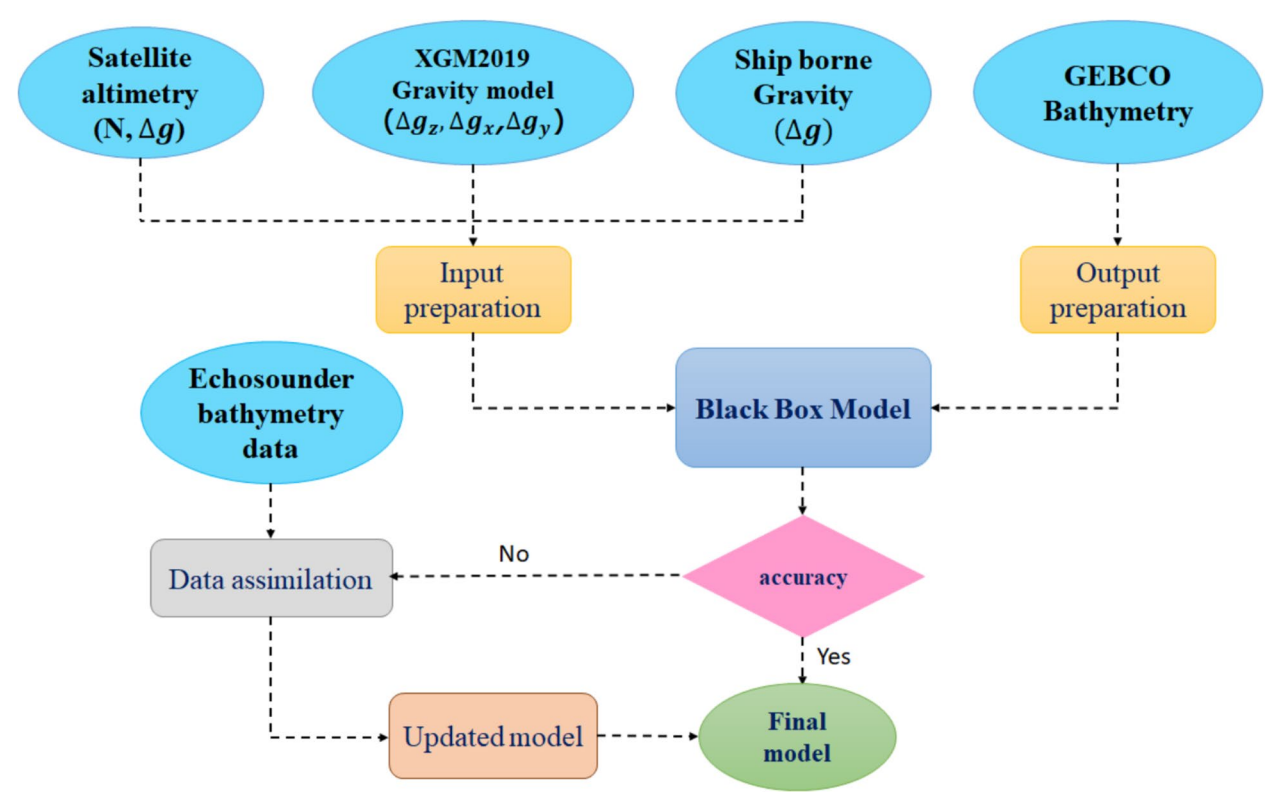


Fig. 2 The flowchart of bathymetry modeling by black-box theory

in neural network models (Raheli et al. 2017; Than et al. 2021). One of the structures often used by researchers in artificial neural networks modeling is the sMultilayer Perceptron Neural Network (MLP). In detail, MLP is a type of feedforward artificial neural network composed of three layers: input, hidden, and output layers (Ren et al. 2020; Blaiech et al. 2012). The input layer takes in the input data, feature processing occurs in the hidden layers, and the output layer displays the predicted outcomes, and the hidden layer can have one or more layers. Initially, identification is performed with single hidden layer, and if the modeling is not responsive, the number of layers will increase. MLP is an enhancement of the standard linear single perceptron. It is particularly effective for tackling classification tasks that map input vectors to one or more groups. By optimizing the weights and thresholds for all nodes, the network can model a wide range of classification functions (Teja And Rao 2011; Palchevsky et al. 2023). Optimization of the weights can be adjusted using the learning algorithm that are classified into supervised and unsupervised ones. In a MLP network,  $\{x_1, x_2, \dots, x_n\}$ as inputs are connected to neuron through weight functions  $\{w_1, w_2, \dots, w_n\}$ . Furthermore, a tunable bias can be incorporated into the neuron which processes these collective inputs, and the output is evaluated against a specific threshold value via the activation function. Sigmoid functions are commonly employed in MLP to add nonlinearity to the model (Pirone et al. 2023; Zhang et al. 2018). A standard feedforward structure for MLP is illustrated in Fig. 3.

Each element of MLP based on Fig. 3 computes by the following relation:

$$y_k = G_q \left( \sum_{i=1}^n w_{qn} x_n + b_q \right), \tag{2}$$

where n is the number of inputs, q the number of neurons in hidden layer, k the number of output that is defined by  $1 \le k \le q$  and  $G_q$  is Log-sigmoid transfer function (logsig) (Suparta And Alhasa 2013; Engström et al. 2020; Koutsellis et al. 2022).

To use MLP, three key points are needed: appropriate training algorithm, optimal number of epochs to avoid the over-train effect, and select the optimal number of neurons to avoid the over-fit effect. In the numerical result section, more details are provided. In this study, the MLP model is organized into a three-layer structure, consisting of an input layer, a single hidden layer, and an output layer. The inputs and outputs include latitude, longitude, geoid height, gravity anomaly, gravity

Mohammad et al. Geoscience Letters (2025) 12:53 Page 6 of 18

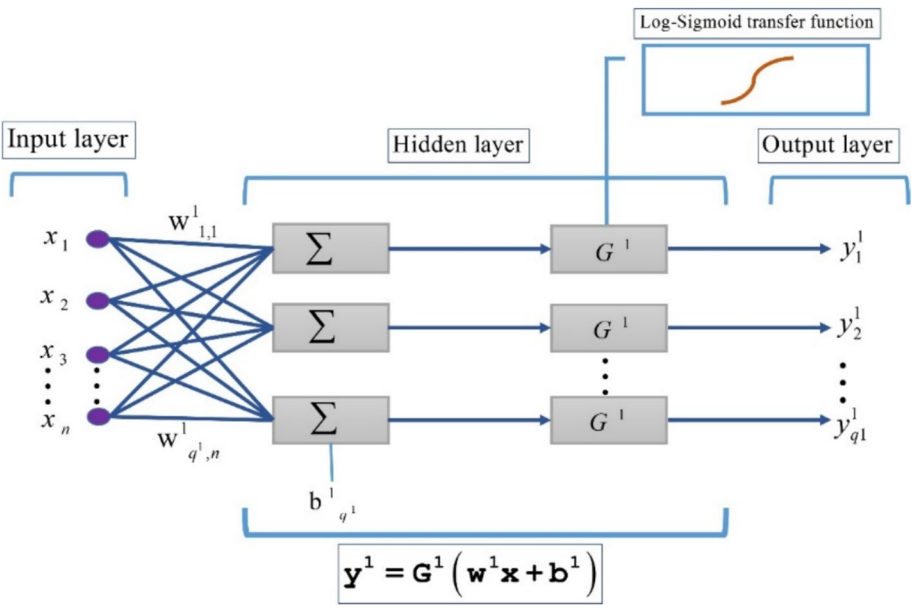


Fig. 3 A typical multi-layer perceptron neural network style used in this study with layers, also 1 refers to the first layer of hidden layer

gradients, and bathymetry, respectively. A log-sigmoid transfer function is used, and the Levenberg–Marquardt algorithm (trainlm) is selected for training the MLP network (Bekas et al. 2021).

#### Adaptive neuro-fuzzy inference system (ANFIS)

The adaptive neuro-fuzzy inference system (ANFIS) integrates two soft computing techniques: artificial neural networks and fuzzy logic (Yang et al. 2019; Zounemat-Kermani et al. 2020). Fuzzy set theory effectively addresses imprecision in decision-making scenarios that involve uncertainty and ambiguity in real-world applications. Fuzzy inference maps input data to an output dataset based on fuzzy set principles. Knowledge is represented through a set of clear linguistic rules that are easily comprehensible for individuals without technical backgrounds. Fuzzy systems can model nonlinear processes using linguistic variables when sufficient knowledge about the system is available. The fuzzy logic component serves as a decision-making tool to manage uncertainties in the decisions made by neural networks (Suparta And Alhasa 2013; Yang et al. 2019).

Figure 4 shows as typical the ANFIS utilizes a Sugeno fuzzy model featuring three inputs, one output, and three rules, organized into five layers. Assume the system has three inputs  $x_1$ ,  $x_2$  and  $x_3$ , three rules, and one output y:

If  $x_1$  is  $A_1$  and  $x_2$  is  $B_1$  and  $x_3$  is  $C_1$ , then  $f_1 = a_1x_1 + b_1x_2 + c_1x_3 + d_1$ .

If  $x_1$  is  $A_2$  and  $x_2$  is  $B_2$  and  $x_3$  is  $C_2$ , then  $f_2 = a_2x_1 + b_2x_2 + c_2x_3 + d_2$ .

If  $x_1$  is  $A_3$  and  $x_2$  is  $B_3$  and  $x_3$  is  $C_3$ , then  $f_3 = a_3x_1 + b_3x_2 + c_3x_3 + d_3$ .

$$w_{i} = \mu_{A_{i}}(x_{1}) \times \mu_{B_{i}}(x_{2}) \times \mu_{C_{i}}(x_{3}), i = 1, 2, 3,$$

$$\overline{w}_{i} = \frac{w_{i}}{w_{1} + w_{2} + w_{3}},$$

$$f = \frac{f_{1}w_{1} + f_{2}w_{2} + f_{3}w_{3}}{w_{1} + w_{2} + w_{3}} = \overline{w}_{1}f_{1} + \overline{w}_{2}f_{2} + \overline{w}_{3}f_{3}.$$
(3)

The first layer serves as the input and fuzzification stage. Each node in this layer represents a fuzzy set, and the output from these nodes indicates the degree of membership, determined by the membership function (MF) of the fuzzy set (Suparta And Alhasa 2013).

Generally, the membership function in the generalized bell MF or Gaussian MF is utilized in the first layer. This layer, known as the rule node, calculates the degree of the membership function (MF) using the AND operator for each rule. Each output node here represents the firing strength of its corresponding rule. The third layer, called the normalization node, performs a normalization process, calculating the ratio of the activity degree of each *i*th rule to the total activation degrees across all rules. The output from this layer is referred to as the normalized firing strength. The fourth layer is responsible for defuzzification, where it computes the consequent parameter values combined with the normalized firing strengths from the previous layer. The final layer, the output node, calculates the weighted average of all incoming signals from the preceding layer (Shoorehdeli et al. 2007). ANFIS employs fuzzy MFs to partition each input dimension, with overlapping MFs allowing multiple local regions to

Mohammad et al. Geoscience Letters (2025) 12:53 Page 7 of 18

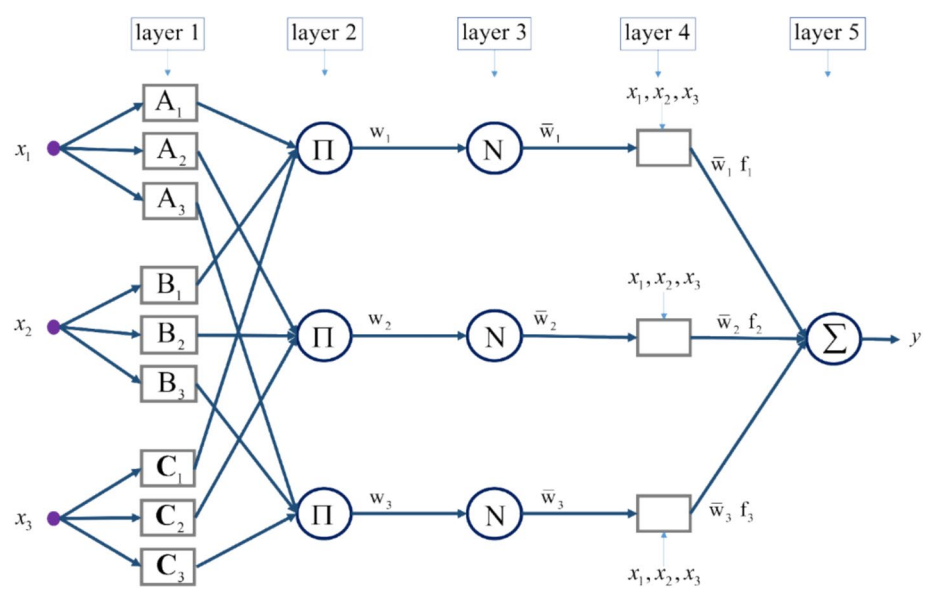


Fig. 4 The architecture of ANFIS

be activated by a single input. Since simple local models are used in the ANFIS framework, its approximation capability depends on how finely the input space is divided, which is influenced by the number of MFs and layers. Typically, bell-shaped MFs are employed, with a maximum value of 1 and a minimum of 0. (Suparta And Alhasa 2013; Pirone et al. 2023; Yang et al. 2019):

$$\mu_{A_i}(x) = \frac{1}{1 + \left[ \left( \frac{x - e_i}{h_i} \right)^2 \right]^{g_i}},\tag{4}$$

where  $\{e_i, g_i, h_i\}$  are the parameters of MFs that influence their shape.

In the ANFIS architecture, the first and fourth layers contain adaptive nodes. To optimize these parameters, a learning algorithm is required. Pirone et al. (2023) developed two learning algorithms: the hybrid learning algorithm and backpropagation. The hybrid learning algorithm combines two approaches: least squares and gradient descent are utilized in this approach, which includes two main stages: forward and backward propagation. In the forward stage, the input to the network moves through to the fourth layer, where the outcome parameters are established using the least squares technique. In the backward stage, once the error is computed, the error signal is sent back, allowing for the adjustment of the premise parameters through the gradient descent method. In this study, as mentioned before, the inputs and output include latitude, longitude, geoid height, gravity anomaly, gravity gradients, and bathymetry. The generalized bell function is used as the membership function, and the hybrid learning algorithm is chosen for training the ANFIS model.

# Local linear model tree (LOLIMOT)

While Neuro-Fuzzy systems have emerged as a compelling and effective data modeling approach by merging the established learning principles of neural networks with the clear interpretability of fuzzy logic, they face challenges related to the curse of dimensionality. To address high-dimensional issues while preserving the beneficial features of Neuro-Fuzzy systems (such as linearity in weights, transparency, and the partition of unity), some method for reducing model complexity is essential to create more parsimonious models. A key consideration for the success of the Local Linear Model Tree (LOLIMOT) is the divide and conquer strategy (Duncanson et al. 2022). As shown by Nelles (2001) among others, LOLI-MOT is an incremental algorithm for constructing trees that partitions the input space using axis-aligned splits. The core concept of locally linear neuro-fuzzy models involves dividing the input space into smaller subspaces defined by fuzzy validity functions. Each resulting linear segment, along with its validity function, can be viewed as a fuzzy neuron. Consequently, the entire model functions as a neuro-fuzzy network with one hidden layer and a linear neuron in the output layer, which computes the weighted sum of the outputs from the locally linear models. The overall output of the network is determined as a weighted sum of the local linear model outputs, where the validity function acts as the weighting factors dependent on the operating point. Typically, the validity

Mohammad et al. Geoscience Letters (2025) 12:53 Page 8 of 18

functions are represented as normalized Gaussian distributions (Duncanson et al. 2022; Nelles 2001). The network structure is illustrated in Fig. 5.

The input–output relationship of locally linear neurofuzzy models is represented in Eq. 5. In this formula Q is the number of neurons,  $x = [x_1, x_2, ..., x_n]^T$  is the model input,n is number of input dimension, N is the number of input samples and the weights  $w_{qn}$  denote the local linear model parameters for q th neuron and n th input (Nelles 2001):

$$\hat{y}_{q} = w_{q0} + w_{q1}x_{1} + w_{q2}x_{2} + \dots + w_{qn}x_{n}, \hat{y} = \sum_{q=1}^{Q} y_{q} \Phi_{q}(\underline{x}).$$
 (5)

The validity functions are selected as normalized Gaussians. Normalization is essential for accurately interpreting these validity functions. The formulation of the validity functions is presented in Eqs. 6 and 7:

$$\Phi_q(\underline{x}) = \frac{\mu_q(\underline{x})}{\sum_{n=1}^{Q} \mu_n(\underline{x})},\tag{6}$$

$$\mu_{q}(\underline{x}) = \exp \begin{pmatrix} \frac{(x_1 - c_{q1})^2}{-2\sigma_{q1}^2} \end{pmatrix} + \exp \begin{pmatrix} \frac{(x_n - c_{qn})^2}{-2\sigma_{qn}^2} \end{pmatrix}.$$

Each Gaussian validity function is defined by two parameters: center  $c_{\rm qn}$  and standard deviation  $\sigma_{\rm qn}$ . Local optimization of linear parameters is achieved using the least squares technique. The corresponding regression matrix for the measured data samples is defined in

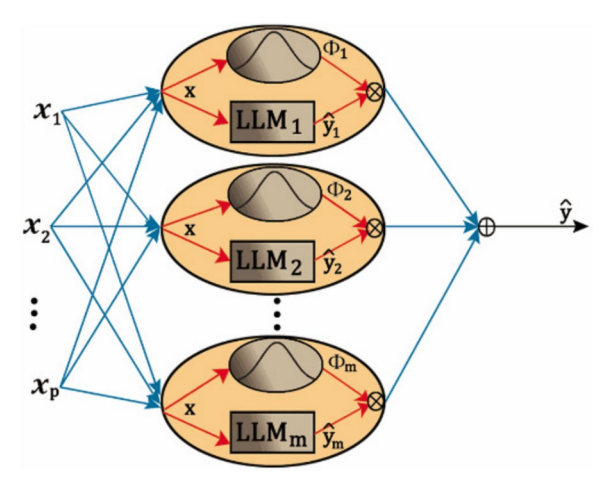


**Fig. 5** Configuration of a static local linear neuro-fuzzy network with **Q** neurons for **N** inputs (Hajian et al. 2012)

Eq. 8. Consequently, the weights can be determined using Eqs. 9 and 10, as illustrated in Eq. 11:

$$X = \begin{bmatrix} 1 & x_1(1) & \cdots & x_n(1) \\ 1 & x_1(2) & \cdots & x_n(2) \\ \vdots & \vdots & \vdots & \vdots \\ 1 & x_1(N) & \cdots & x_n(N) \end{bmatrix},$$
 (8)

$$P_{q} = \begin{bmatrix} \Phi_{q}(\underline{x}(1)) & 0 & 0 & 0\\ 0 & \Phi_{q}(\underline{x}(2)) & 0 & 0\\ \vdots & \vdots & \vdots & \vdots\\ 0 & 0 & 0 & \Phi_{q}(\underline{x}(N)) \end{bmatrix}, \tag{9}$$

$$W_q = [w_{q0}, w_{q1}, w_{q2}, \dots, w_{qn}]^T,$$
(10)

and

$$\hat{y}_q = X\hat{W}_q; \ \hat{W}_q = \left(X^T P_q X\right)^{-1} X^T P_q y_q.$$
 (11)

LOLIMOT is an incremental algorithm that consists of three iterative steps. First, the least effective Local Linear Model is identified based on local loss functions, and this LLM neuron is chosen for division. In the second step, all potential divisions of this LLM in the input space are generated and evaluated (Schwingshackl et al. 2017). Figure 6 illustrates the first five iterations of the LOLIMOT algorithm applied to a two-dimensional input space.

# **Data fusion**

In order to improve the mathematical modeling of bathymetry by local data, the 3DVAR method is used in this study (Teruzzi et al. 2014). This method provides the optimal estimate of the bathymetry via the minimization of the following cost function (Pirooznia et al. 2024, 2023):

$$J = \frac{1}{2} \left( x - x^b \right)^T B^{-1} \left( x - x^b \right)$$

$$+ \frac{1}{2} \left( y - A x^b \right)^T R^{-1} \left( y - A x^b \right)$$

$$x = x^b + W \left( y - A x^b \right)$$

$$W = BA^T \left( ABA^T + R \right)^{-1},$$
(12)

where x is the state vector which includes the improved bathymetry,  $x^b$  is the bathymetry derived by basic model, A is coefficient matrix, B is the variance covariance matrix of model and R is the variance covariance matrix of observations. Here the matrix B is the covariance matrix of the estimated bathymetry using the black-box model, and it is estimated by using the MSEs obtained from the model as the diagonal elements, while

Mohammad et al. Geoscience Letters (2025) 12:53 Page 9 of 18

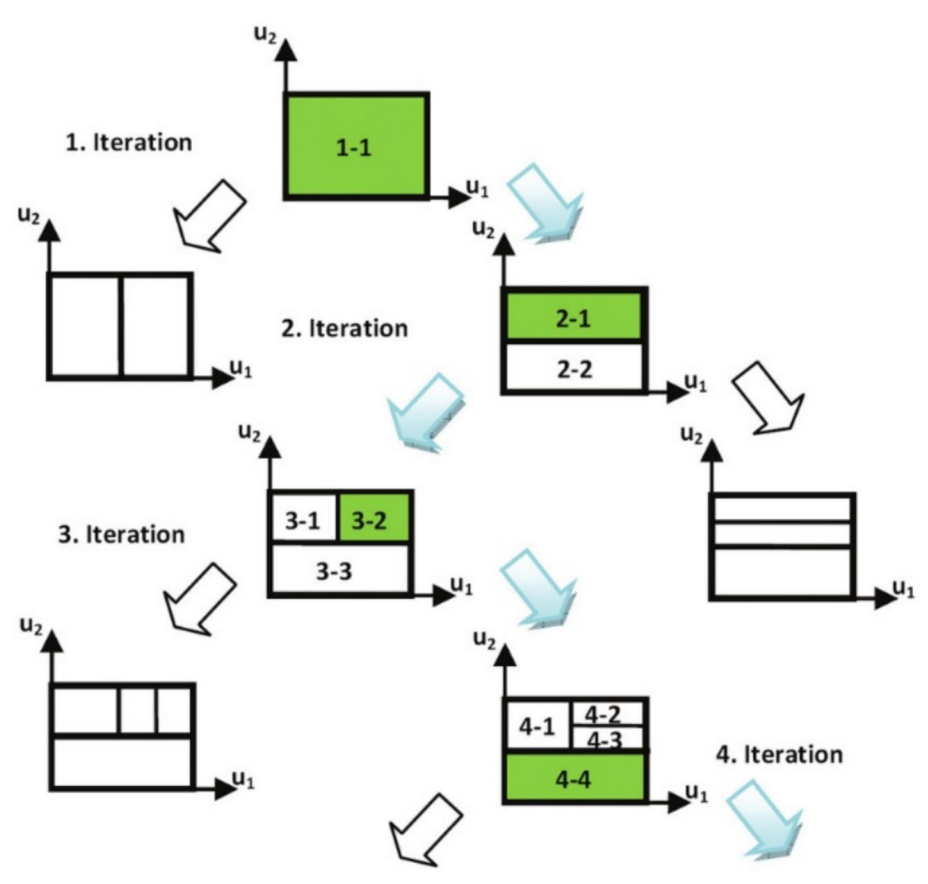


Fig. 6 Functioning of the LOLIMOT algorithm during the initial five iterations for a two-dimensional input space

the off-diagonal covariance is empirically approximated through multiple runs of the model with different initial weights.

Also the matrix R is the covariance matrix of the echo sounder observations, in the first-order approximation forms a diagonal matrix, where the diagonal elements represent the instrument precision.

As mentioned before, the nonlinear physical relation as an inverse problem between gravity field parameters such as geoid height, gravity anomaly, and gravity gradients with bathymetry and the difficulty in reaching a deterministic solution has been proven (Fan et al. 2021). Therefore, an alternative data-driven method based on artificial intelligence algorithms is proposed to model bathymetry. In this regard, the input of the artificial intelligence algorithms is geoid height determined by satellite altimetry, gravity gradients of the XGM2019e gravity model, and gravity anomaly data derived from altimetry and shipborne measurements. The output of the model is the bathymetry of GEBCO.

By preparing the above input and output data sets, the aim is to identify the model between the input and output. Generally, two main steps are done for modeling bathymetry. The first is the identification of appropriate artificial intelligence algorithms, such as MLP, ANFIS, and LOLIMOT, for modeling bathymetry in the Persian Gulf and Oman Sea. The second step is improving the bathymetry model by data fusion of in situ bathymetry data.

#### Modeling procedure

# MLP modeling

In general, in order to identify the model using the MLP, it is necessary to consider the following items:

 Dividing input and output data into two parts: train and test.

To this end, 70% of the data is given as train data for training the MLP network, and 30% of the data is selected as test data for checking.

Mohammad et al. Geoscience Letters (2025) 12:53 Page 10 of 18

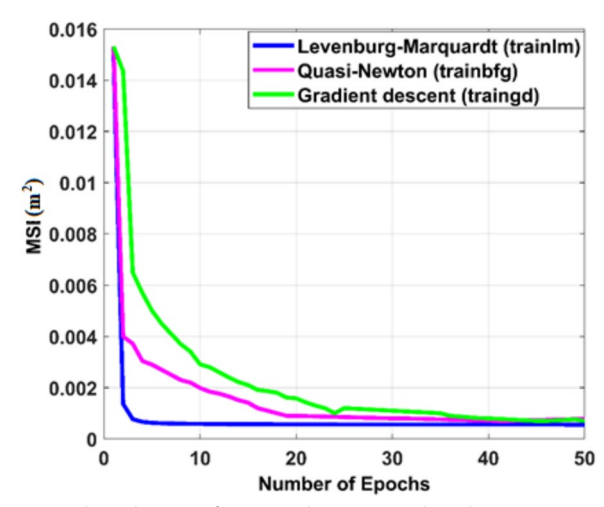


Fig. 7 Show the MSE of train to select training algorithm

 If necessary, input and output data will be normalized.

Inputs and output data are checked, and if the range of inputs and output data are not the same, data will be normalized.

iii. Select the training algorithm.

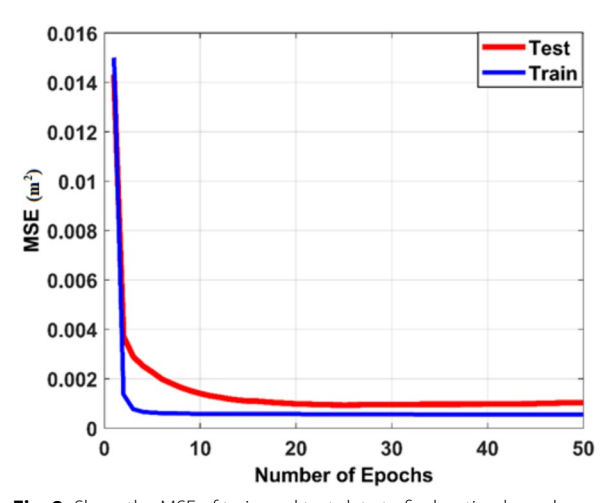
To do this, the MSE graph of train and test data with regard to the number of epochs is drawn, and the slope of the convergence of the graph is examined; the optimization algorithms that have the fastest convergence are chosen as the training algorithm. As shown in Fig. 7 Levenberg—Marquardt algorithm (trainlm) with a learning rate of 0.01 is selected for training the MLP network.

iv. Select the optimal number of epochs to avoid the over-train effect.

To find the optimal number of epochs in the MLP network, the number of epochs increases step by step, and the MSE graph for train and test data is drawn. The point where, by increasing the number of epochs, the MSE of train and test data stays constant corresponds to the optimal number of training epochs. As shown in Figure 8, the optimal number of epochs is obtained 10.

v. Select the optimal number of neurons to avoid the overfit effect.

To find the optimal number of neurons in the MLP network, the number of neurons increases step by step, and MSE graphs for train and test data are drawn together. The point where the smallest MSE for train and test data is obtained corresponds to the optimal number of neurons. As



 $\begin{tabular}{ll} \textbf{Fig. 8} & \textbf{Show the MSE of train and test data to find optimal number of epochs} \\ \end{tabular}$ 

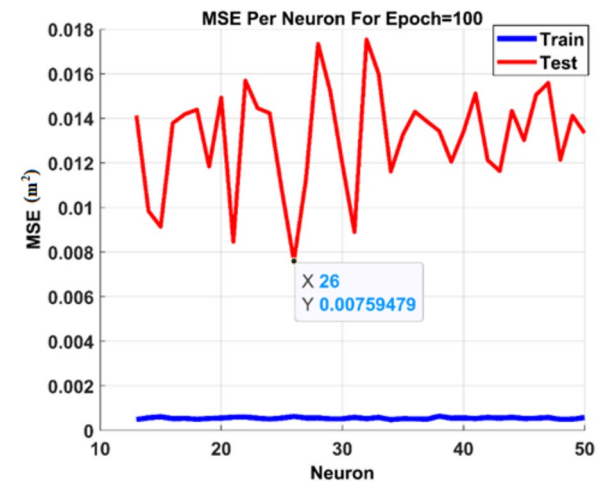


**Fig. 9** Show the MSE of train and test data to find optimal number of neurons

shown in Figure 9, the optimal number of neurons is obtained as 26. Finally, the MLP modeling process is done after training the MLP network by considering appropriate neurons and epochs. Figure 10 shows the bathymetry modeling using the MLP network with 84.55% fitting on test data.

# ANFIS modeling

In general, similar to MLP, in order to identify the model using the ANFIS, it is necessary to consider the following items:

i. Dividing input and output data into two parts: train and test.

Mohammad et al. Geoscience Letters (2025) 12:53 Page 11 of 18

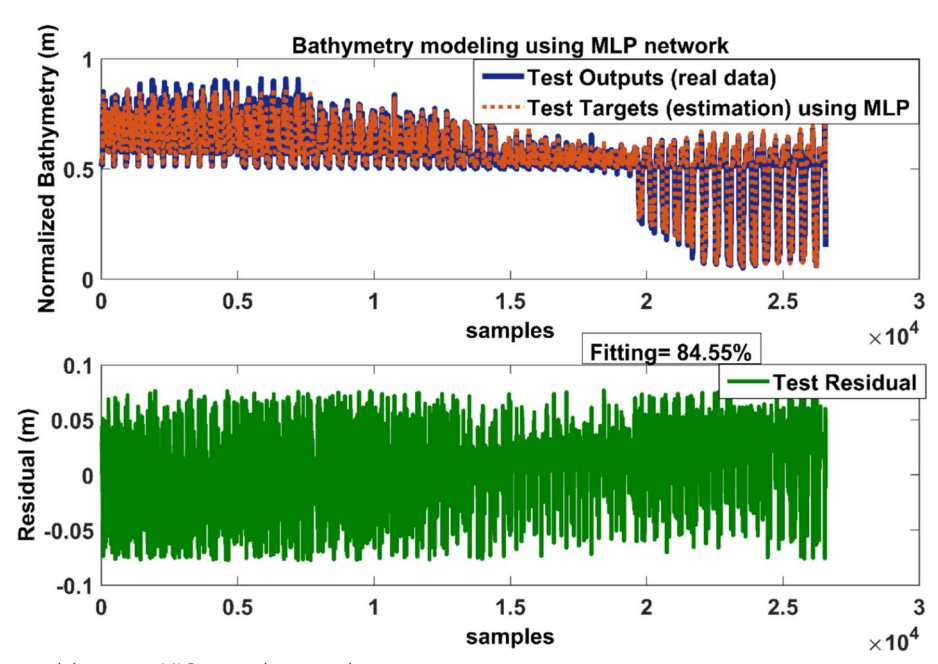


Fig. 10 Bathymetry modeling using MLP network on test data

To this end, 70% of the data is given as train data for training the ANFIS, and 30% of the data is selected as test data for checking.

 If necessary, input and output data will be normalized.

Input and output data are checked, and if the range of input and output data is not the same, data will be normalized.

iii. Determination the optimal number of membership functions (MFs).

To find the optimal number of MFs, the number of MFs is increased step by step, and the MSE graph for train and test data is drawn together. The point where the lowest MSE for train and test data is obtained corresponds to the optimal MFs. In this study, the number of optimal MFs is obtained as 3.

iv. Select the optimal number of epochs to avoid the over-train effect.

Similar to the previous section, to find the optimal number of epochs, the number of epochs increases step by step, and the MSE graph for train and test data is drawn together. The point where, by increasing the number of epochs, the MSE of train and test data stays constant marks the optimal training epoch. In this study, the optimal number of epochs is obtained from 15.

Finally, Fig. 11 shows the bathymetry modeling using ANFIS network with 84.76% fitting on test data.

# LOLIMOT modeling

As for the previous two modeling cases, in order to use LOLIMOT, it is necessary to consider: Similar to previous modeling, dividing input and output data into two parts of train and test, normalizing the input and output data, and selecting the optimal number of epochs and neurons. Here, modeling with consideration of spatial analysis using the LOLIMOT is explained in more detail. Figure 12 shows bathymetry modeling using LOLIMOT on test data with 90.64% fitting.

In summary, the purpose of step 1 includes:

- View full details of determination the structure of input—output model
- Bathymetry modeling in the Persian Gulf and Oman Sea
- Using this model obtained in the next step for data fusion.

# Results and analysis

Based on the model structures identified in the previous section, the LOLIMOT model demonstrated superior accuracy and was therefore selected as the basic model for the results. Due to the low quality of input and output data for the modeling procedure, including altimeter-derived geoid height and gravity anomaly data, as well as available limitations in gravity gradients via the

Mohammad et al. Geoscience Letters (2025) 12:53 Page 12 of 18

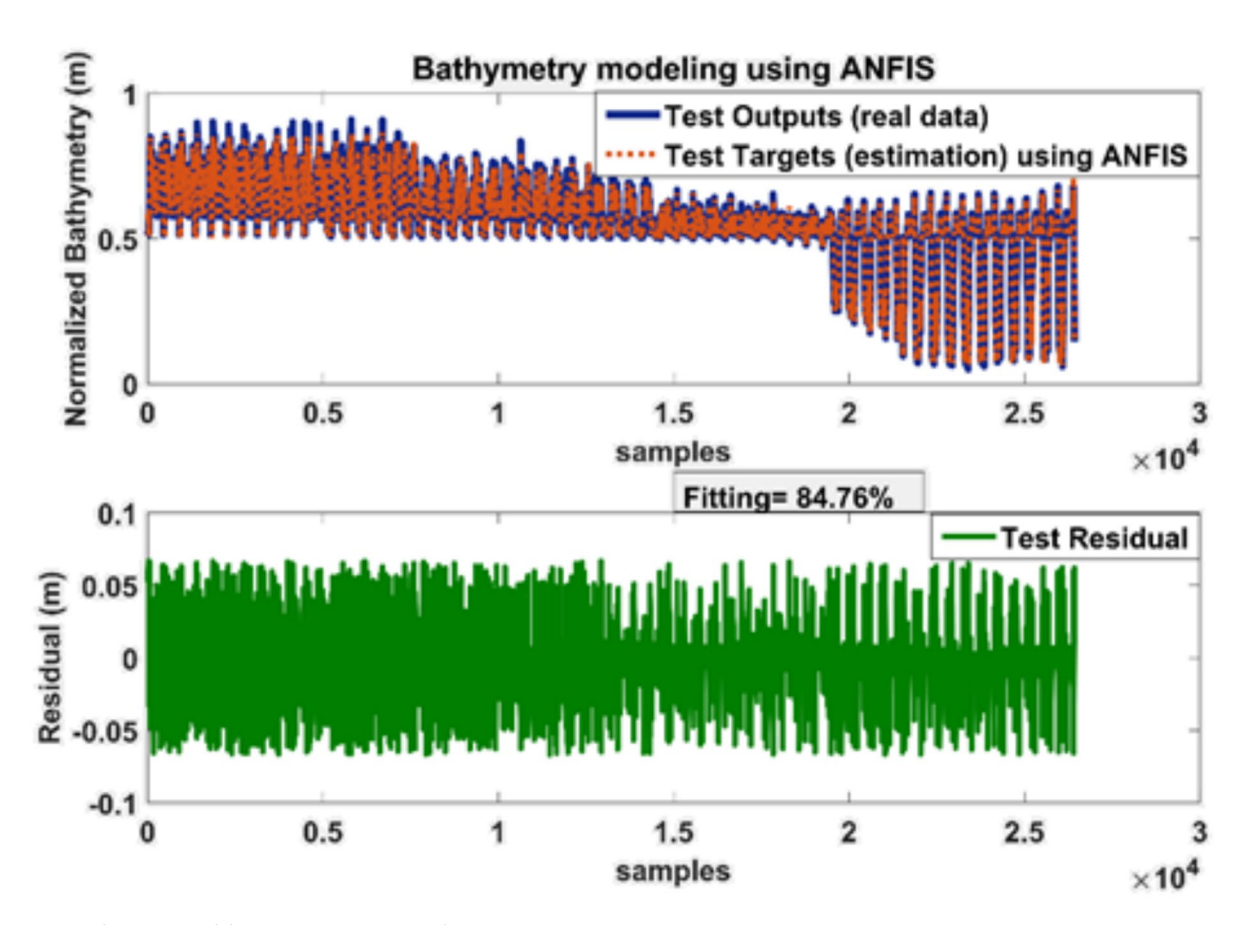


Fig. 11 Bathymetry modeling using ANFIS on test data

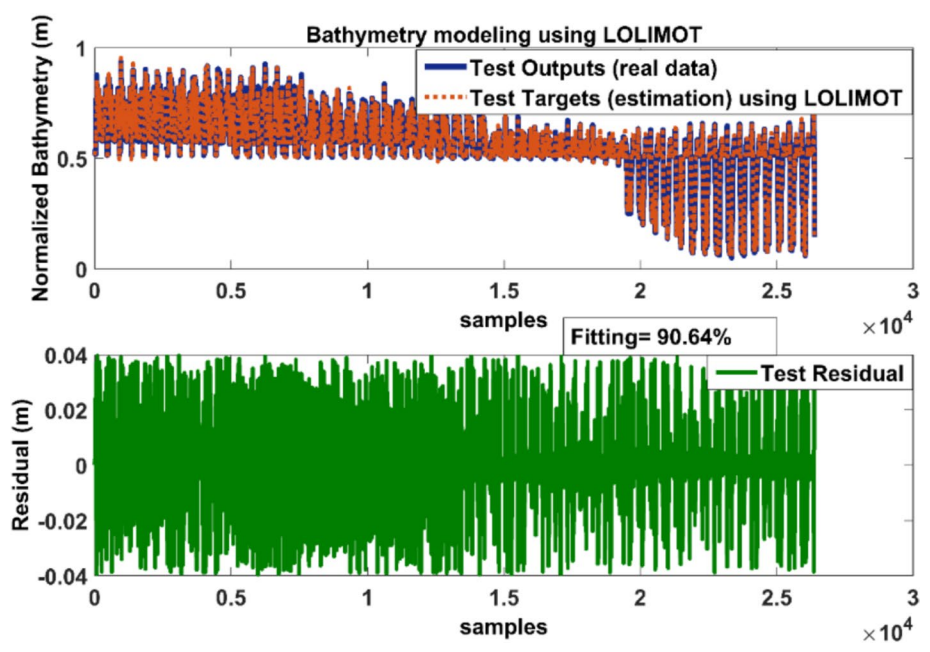


Fig. 12 Bathymetry modeling using LOLIMOT on test data

Mohammad et al. Geoscience Letters (2025) 12:53 Page 13 of 18

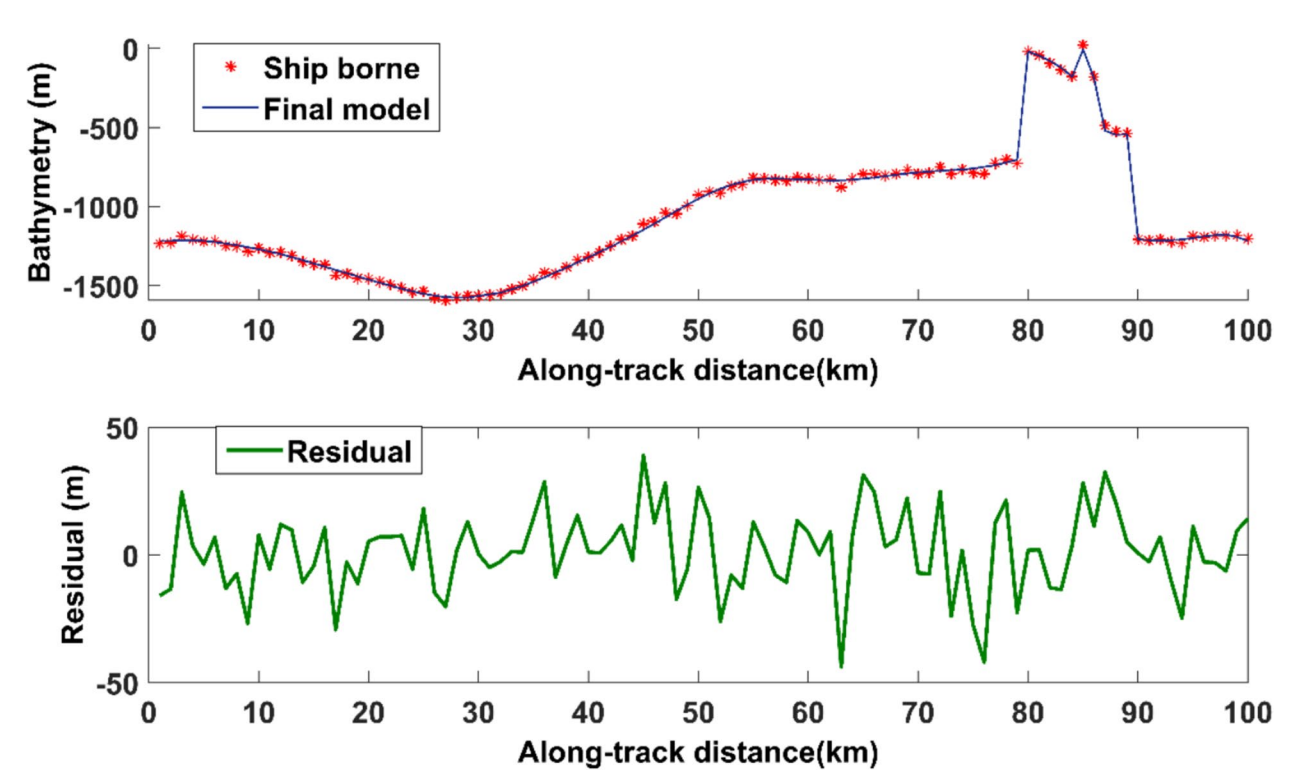


Fig. 13 A typical comparison of shipborne bathymetry and final model along-track in Chabahar region

XGM2019e global gravity model and GEBCO bathymetry used in the basic model, the results are affected by the accuracy of the input and output data, particularly in shallow water (Hwang 1998), data fusion is used to improve the basic model via in situ observations.

To this end, we have three types of bathymetries in Chabahar, Genaveh, and Alamshah regions: (i) bathymetry observed from shipborne measurements; (ii) bathymetry obtained from a basic model; and (iii) bathymetry from the global GEBCO model. To validate the final model extracted from data fusion, two tracks of bathymetry measured by echo sounder are not involved in computations, only used for comparison and checkpoints. Figure 13 shows a typical comparison between the final model and shipborne bathymetry along a track profile in the Chabahar region. The comparison between the final model and the ship-based bathymetry measurements in the regions of Chabahar, Genaveh, and Alamshah (a control track that was not used in the data fusion process) resulted in RMSE values of approximately 4 m, 0.8 m, and 0.92 m, respectively. Prior to the data fusion, the RMSE values were 6 m, 2.5 m, and 2 m, respectively, in those same regions. It indicates that the final model cannot fully reproduce the shipborne bathymetry used. Other studies have also confirmed this. See the results of Smith et al. (2005), Smith and Moose (1997), and Vrdoljak and Bašić (2023). The final model can extract the majority of high-frequency seabed features like seamounts, but it still has large oscillations due to the lack of shipborne bathymetry, low accuracy of satellite altimetry, and existing restrictions of global gravity models in coastal areas. Over the deep parts of the ocean, due to the increasing accuracy of satellite altimetry, the modeled and shipborne bathymetry agree very well. In Chabahar, Genaveh, and Alamshah regions, reefs and hills are seen in the final model. Figure 14 shows the final model in Chabahar, Genaveh, and Alamshah regions using data fusion. This model can utilize the data to generate bathymetry. Moreover, the final model needs to be appropriately adjusted to account for abrupt changes in subsurface geology in offshore areas. The availability of higher-resolution altimeter data could enhance bathymetric predictions.

### Discussion

As we know, the traditional approaches to bathymetry modeling have primarily relied on well-established formulas, such as the Parker model. The Parker mathematical formula is based on parameters like the density difference between seawater and seafloor, the mean thickness of the crust, the mean depth of seawater, and the densities of the Earth's mantle and crust. However, these methods face inherent difficulties, including the lack of adequate knowledge for accurately estimating the model

Mohammad et al. Geoscience Letters (2025) 12:53 Page 14 of 18

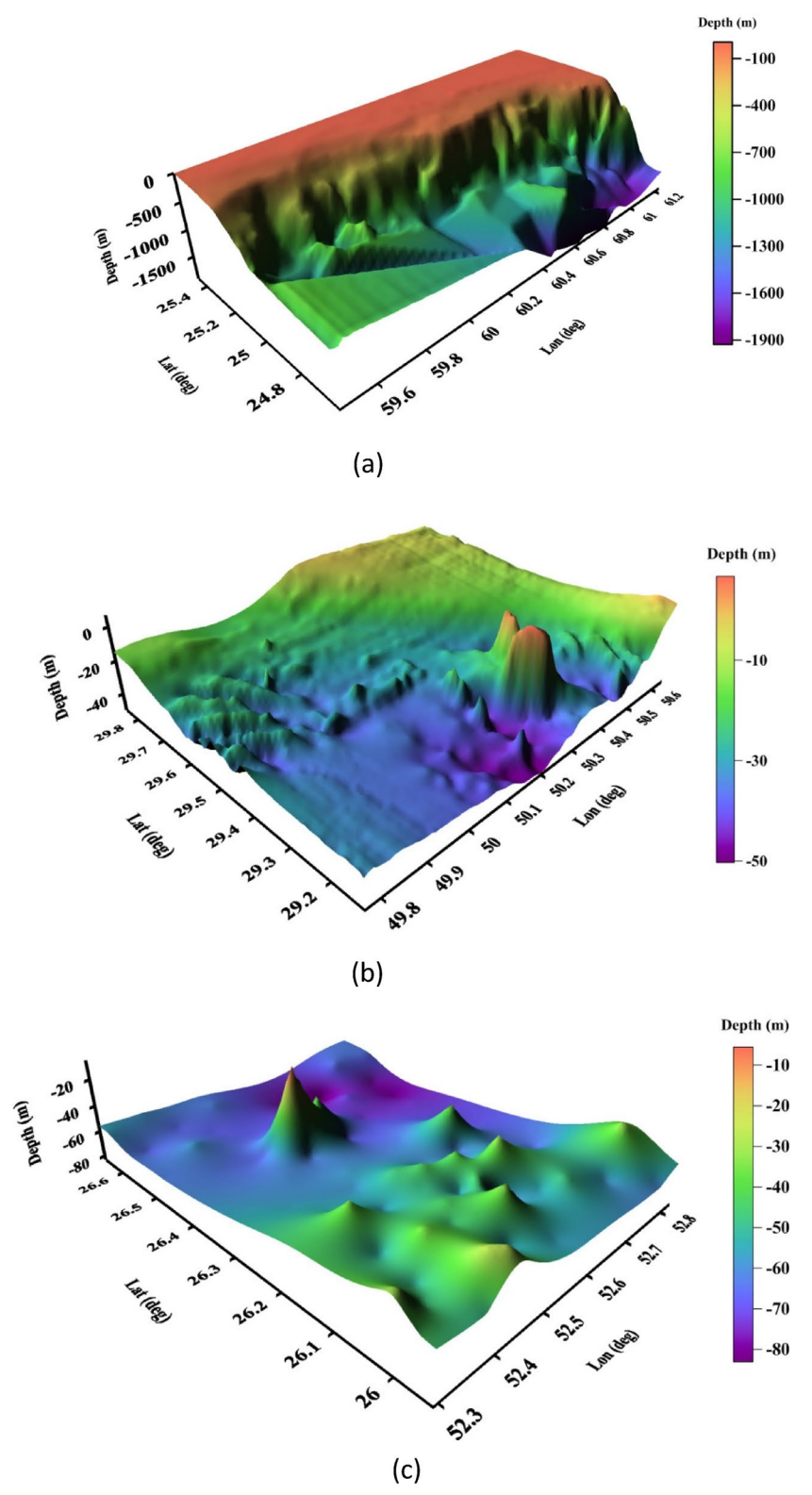


Fig. 14 The final model in Chabahar (a), Genaveh (b), and Alamshah (c) regions using data fusion

Mohammad et al. Geoscience Letters (2025) 12:53

parameters and the use of linearized approximations in the implementation process, leading to potential bias and computational errors. Furthermore, the determination of bathymetry from gravity anomaly is essentially an inverse problem, which is considered an ill-posed problem. The solution to this inverse problem may not be unique and can be unstable, necessitating the use of regularization techniques to overcome these challenges.

Nowadays, unlike the past where we sought appropriate ways to solve complex and difficult equations, we are dealing with a vast amount of data, which has led us to focus more on data analysis and processing. With the emergence of artificial intelligence, the modeling tools have shifted from physical to mathematical approaches. In this context, an alternative method for bathymetry modeling is presented, which has its own advantages and disadvantages. The main advantage of the proposed approach is its flexibility and high speed, which allows considering various input parameters. The significant challenge of this method is its strong dependence on the input data, which must be accurate. Therefore, it requires careful monitoring and quality control of the input data to ensure reliable results. Moreover, there are also some computational complexities dealing with overfitting and overtraining phenomena as well as selecting the best and fastest training algorithm.

The present study demonstrates the effectiveness of combining multiple gravity data sources with black-box modeling techniques for bathymetry estimation. Compared to traditional approaches, this method allows for better representation of nonlinear relationships between gravity parameters and seafloor topography.

While previous studies have applied similar approaches, our work emphasizes the advantages of integrating satellite altimetry, gravimetry, and shipborne data to enhance accuracy, particularly in regions with limited observations. In contrast to earlier research that typically relied on a single model, this study evaluates three blackbox modeling techniques (MLP, ANFIS, and LOLIMOT) as the primary models and further assimilates observational shipborne bathymetry through 3D variational optimization. This combined strategy leads to improved local accuracy and resolution. Moreover, lessons learned from earlier studies informed the selection of input parameters, model architecture, and data assimilation strategies in our research.

Among the limitations, satellite altimetry measurements in coastal areas are influenced by the waveform, which adheres to the Brown model in open waters. In coastal zones, factors like shallow depths complicate this model, causing errors in range determination; thus, the retracking correction available in the geophysical data records (GDR) file has been applied to

observations up to 10 km from the shore. Moreover, the accuracy of gravity data derived from satellite altimetry decreases significantly near coastal regions due to contamination by land signals and complex hydrodynamic conditions. In contrast, shipborne gravimetry data generally provide higher accuracy, although they may still be affected by local environmental factors. To mitigate these effects, artificial intelligence techniques have been employed to assign higher weights to in situ shipborne measurements and gravity model data in coastal regions. Despite these measures, the accuracy of depth estimation in coastal areas remains lower than that achieved in offshore regions.

These improved local and regional bathymetry predictions provide valuable datasets that can support the refinement of global bathymetry models such as ETOPO5. This study shows that carefully combining global and local information, while accounting for coastal corrections, contributes to both practical applications and the advancement of oceanographic modeling techniques.

#### **Conclusions**

The study presents a novel scheme for regional bathymetry modeling in the Persian Gulf and Oman Sea using a data-driven approach based on black-box theory. The proposed methodology utilizes geodetic data sources such as satellite altimetry, gravity model, and shipborne gravity data as inputs to train nonlinear black-box models like MLP, ANFIS, and LOLIMOT. The results demonstrate the effectiveness of the proposed approach, with the LOLIMOT model exhibiting the highest accuracy among the tested algorithms, achieving a fitting of 90.64% on the test data. To further improve the bathymetry model, the study incorporated in situ shipborne bathymetry measurements using a 3D variational optimization method. The comparison between the final model and the shipborne bathymetry in control tracks yielded root mean square errors (RMSEs) of around 4 m, 0.8 m, and 0.92 m for the Chabahar, Genaveh, and Alamshah regions, respectively, showcasing the accuracy and reliability of the proposed methodology. The study highlights the importance of incorporating both geodetic and in situ data sources to develop accurate and reliable bathymetry models. The proposed approach can be valuable for a variety of applications, including physical oceanography, marine geology, and ecohydraulics, where detailed knowledge of regional bathymetry patterns is crucial. The study's findings contribute to the ongoing efforts to improve the understanding of ocean processes and support sustainable marine resource management.

Mohammad et al. Geoscience Letters (2025) 12:53 Page 16 of 18

#### **Author contributions**

Conceptualization, M.P., M.A.M.; formal analysis, M.P., M.A.M, I.J., and M.G.; writing—original draft, M.P., M.A.M, I.J., and S.J.; supervision—review and editing, M.P., M.A.M, I.J., and S.J. All authors have read and agreed to the published version of the manuscript.

#### Funding

This research was supported by the Henan Provincial Department of Education "Double First-Class" Project (Grant No. 760507/033).

#### Data availability

In this research, Geophysical Data Records (GDR) of satellite altimetry missions can be accessed from the European Space Agency data services (https://www.esa.int) and AVISO (https://www.aviso.altimetry.fr/en/home.html). Shipborne gravimetry data can be obtained from the Bureau Gravimetrique International (BGI) data services (https://bgi.obs-mip.fr/data-products/gravity-databases/marine-gravity-datas). The XGM2019e gravity model is archived by Zingerle et al. (2020) ( https://doi.org/10.1007/s00190-020-01398-0). For data from the global gridded bathymetry model (GEBCO), refer to (https://www.gebco.net/data\_and\_products/gridded\_bathymetry\_data/). Local bathymetry data are available from the National Geographic Organization or the National Mapping Organization. Global MDT models can be accessed from altimetry product sites such as AVISO (https://www.aviso.altimetry.fr/en/home.html).

#### **Declarations**

#### Competing interests

The authors declare no competing interests.

Received: 28 December 2024 Accepted: 10 October 2025 Published online: 22 October 2025

#### References

- Abulaitijiang A, Andersen OB, Sandwell D (2019) Improved Arctic Ocean bathymetry derived from DTU17 gravity model. Earth Space Sci 6(8):1336–1347. https://doi.org/10.1029/2018EA000502
- An X, Zhang Y, Li J, Wang H (2022) Improved gravity-geologic method reliably removing the long-wavelength gravity effect of regional seafloor topography: a case of bathymetric prediction in the South China Sea. IEEE Trans Geosci Remote Sens 60:4211912. https://doi.org/10.1109/TGRS. 2022.3223047
- Bekas GK, Alexakis DE, Gamvroula DE (2021) Forecasting discharge rate and chloride content of karstic spring water by applying the Levenberg–Marquardt algorithm. Environ Earth Sci 80(11):404. https://doi.org/10.1007/s12665-021-09685-5
- Blaiech A, Khalifa KB, Boubaker M, Bedoui M (2012) Implementation of a multilayer Perceptron Neural networks in multi-width fixed point coding. Int J Mod Optimiz. https://doi.org/10.7763/ijmo.2012.v2.127
- Chen X, Lee RM, Dwivedi D, Son K, Fang Y, Zhang X, Graham E, Stegen G, Fisher JB, Moulton D, Scheibe TD (2021) Integrating field observations and process-based modeling to predict watershed water quality under environmental perturbations. J Hydrol 602:125762. https://doi.org/10.1016/j.jhydrol.2020.125762
- Dick H, Lin J, Schouten H (2003) An ultraslow-spreading class of ocean ridge. Nature 426:405–412. https://doi.org/10.1038/nature02128
- Duncanson L, Kellner JR, Armston J, Dubayah R, Minor DM, Hancock S, Healey SP, Patterson PJ, Saarela S, Marselis S, Silva CE, Bruening J, Goetz SJ, Tang H, Hofton M, Blair B, Luthcke S, Fatoyinbo L, Abernethy K, Alonso A, Andersen, Aplin H-EP, Baker TR, Barbier N, Bastin JF, Biber P, Boeckx P, Bogaert J, Boschetti L, Boucher PB, Boyd DS, Burslem DFRP, Calvo-Rodriguez S, Chave J, Chazdon RL, Clark DB, Clark DA, Cohen WB, Coomes DA, Corona P, Cushman KC, Cutler MEJ, Dalling JW, Dalponte M, Dash J, de-Miguel S, Deng S, Ellis PW, Erasmus B, Fekety PA, Fernandez-Landa A, Ferraz A, Fischer R, Fisher AG, García-Abril A, Gobakken T, Hacker JM, Heurich M, Hill RA, Hopkinson C, Huang H, Hubbell SP, Hudak AT, Huth A, Imbach B, Jeffery KJ, Katoh M, Kearsley E, Kenfack D, Kljun N, Knapp N, Král K, Krůček M, Labrière N, Lewis SL, Longo M, Lucas RM, Main R,

- Manzanera JA, Vásquez Martínez R, Mathieu R, Memiaghe H, Meyer V, Monteagudo Mendoza A, Monerris A, Montesano P, Morsdorf F, Næsset E, Naidoo L, Nilus R, O'Brien M, Orwig DA, Papathanassiou K, Parker G, Philipson C, Phillips OL, Pisek J, Poulsen JR, Pretzsch H, Rüdiger C, Saatchi S, Sanchez-Azofeifa A, Sanchez-Lopez N, Scholes R, Silva CA, Simard M, Skidmore A, Stereńczak K, Tanase M, Torresan C, Valbuena R, Verbeeck H, Vrska T, Wessels K, White JC, White LJT, Zahabu E, Zgraggen C (2022) Aboveground biomass density models for NASA's Global Ecosystem Dynamics Investigation (GEDI) lidar mission. Remote Sens Environ 270:112845. https://doi.org/10.1016/j.rse.2022.113180
- Engström A, Jakobsson L, Orlich M (2020) Explicit Boij-Söderberg theory of ideals from a graph isomorphism reduction. J Pure Appl Algebra 224(11):106405. https://doi.org/10.1016/j.jpaa.2020.106405
- Fan D, Li S, Li X, Yang J, Wan X (2021) Seafloor topography estimation from gravity anomaly and vertical gravity gradient using nonlinear iterative least square method. Remote Sens 13:64. https://doi.org/10.3390/rs130
- Ge X, Wang L, Liu Y, Zhang Z (2025) Seafloor topography inversion from multisource marine gravity data using multi-channel convolutional neural network. Eng Appl Artif Intell 139:109567. https://doi.org/10.1016/j.engap
- Hajian A, Zomorrodian H, Styles P, Greco F, Lucas C (2012) Depth estimation of cavities from microgravity data using a new approach: the local linear model tree (LOLIMOT). Near Surf Geophys 10:221–234. https://doi.org/10.3997/1873-0604.2011039
- Hossain S, Gupta SS, Kwon TH, Kim KD (2021) Derivation and validation of grey-box models to estimate noninvasive in-vivo percentage glycated hemoglobin using digital volume pulse waveform. Sci Rep 11(1):12169. https://doi.org/10.1038/s41598-021-91527-2
- Hwang C (1998) Inverse vening meinesz formula and deflection-geoid formula: applications to the predictions of gravity and geoid over the South China Sea. J Geod 72:304–312. https://doi.org/10.1007/s001900050169
- Jin SG, Camps A, Jia Y, Wang F, Martin-Neira M, Huang F, Yan Q, Zhang S, Li Z, Edokossi K, Yang D, Xiao Z, Ma Z, Bai W (2024) Remote sensing and its applications using GNSS reflected signals: advances and prospects. Satell Navig 5:19. https://doi.org/10.1186/s43020-024-00139-4
- Kiamehr R, Eshagh M (2008) EGMlab a scientific software for determining the gravity and gradient components from global geopotential models. Earth Sci Inform 1:93–103. https://doi.org/10.1007/s12145-008-0013-4
- Knudsen P, Andersen OB (2012) A global mean ocean circulation estimation using goce gravity models-the DTU12MDT mean dynamic topography model. In: 20 years of progress in radar altimetry symposium
- Koutsellis T, Xexakis G, Koasidis K, Nikas A, Doukas H (2022) Parameter analysis for sigmoid and hyperbolic transfer functions of fuzzy cognitive maps. Oper Res 22(5):5733–5763. https://doi.org/10.1007/s12351-022-00717-x
- Lecours V, Dolan MF, Micallef A, Lucieer VL (2016) A review of marine geomorphometry, the quantitative study of the seafloor. Hydrol Earth Syst Sci 20(8):3207–3244. https://doi.org/10.5194/hess-20-3207-2016
- Lei J, Schaefer R, Colarusso P, Novak A, Simpson JC, Masqué P, Nepf HM (2023) Spatial heterogeneity in sediment and carbon accretion rates within a seagrass meadow correlated with the hydrodynamic intensity. Sci Total Environ 854:158685. https://doi.org/10.1016/j.scitotenv.2022.158685
- Ma B, Wu Z, Hu C, Wang H, Xu H, Yan D (2022) Process-oriented SWMM real-time correction and urban flood dynamic simulation. J Hydrol 605:127269. https://doi.org/10.1016/j.jhydrol.2021.127269
- Majumdar TJ, Chander S (2011) Simulation of SARAL (satellite with ARgos and ALtika) resolution gravity over the western Indian offshore for geological/structural interpretation. Geocarto Int 26(1):21–34. https://doi.org/10.1080/10106049.2010.535617
- Mitchell RN, Zhang N, Salminen J, Liu Y, Spencer CJ, Steinberger B, Murphy B, Li ZX (2021) The supercontinent cycle. Nat Rev Earth Environ 2(5):358–374. https://doi.org/10.1038/s43017-021-00160-0
- Nelles O (2001) Nonlinear local optimization. Nonl Syst Identif. https://doi.org/ 10.1007/978-3-662-04323-3\_4
- Oldenburg DW (1974) The inversion and interpretation of gravity anomalies. Geophysics 39(4):526–536
- Olive JA, Behn MD, Ito G, Buck WR, Escartín J, Howell S (2015) Sensitivity of seafloor bathymetry to climate-driven fluctuations in mid-ocean ridge magma supply. Science 350(6258):310–313. https://doi.org/10.1126/science.aad0715

- Palchevsky E, Antonov V, Enikeev R, Breikin T (2023) A system based on an artificial neural network of the second generation for decision support in especially significant situations. J Hydrol 616:128844. https://doi.org/10.1016/j.jhydrol.2022.128844
- Parker RL (1973) The rapid calculation of potential anomalies. Geophys J Int 31:447–455. https://doi.org/10.1111/j.1365-246X.1973.tb06513.x
- Peng Q, Xie SP, Wang D, Huang RX, Chen G, Shu Y, Shi J-R, Liu W (2022) Surface warming–induced global acceleration of upper ocean currents. Sci Adv 8(16):eabj8394. https://doi.org/10.1126/sciadv.abj839
- Petrovskaya MS, Vershkov AN (2006) Non-singular expressions for the gravity gradients in the local north-oriented and orbital references frames. J Geod 80:117–127
- Pirone D, Cimorelli L, Del Giudice G, Pianese D (2023) Short-term rainfall forecasting using cumulative precipitation fields from station data: a probabilistic machine learning approach. J Hydrol. https://doi.org/10.1016/j.jhydrol.2022.128949
- Pirooznia M, Emadi SR, Alamdari MN (2016) The time series spectral analysis of satellite altimetry and coastal tide gauges and tide modeling in the coast of Caspian sea. Open J Mar Sci 6:258–269. https://doi.org/10.4236/ojms. 2016 62021
- Pirooznia M, Raoofian Naeeni M, Tourian MJ (2023) Modeling total surface current in the Persian Gulf and the Oman Sea by combination of geodetic and hydrographic observations and assimilation with in situ current meter data. Acta Geophys 71:2839–2863. https://doi.org/10.1007/s11600-022-00985-3
- Pirooznia M, Voosoghi B, Poreh D, Amini A (2024) Integrating hydrography observations and geodetic data for enhanced dynamic topography estimation. Remote Sens 16:527. https://doi.org/10.3390/rs16030527
- Raheli B, Aalami MT, El-Shafie A, Ghorbani MA, Deo RC (2017) Uncertainty assessment of the multilayer perceptron (MLP) neural network model with implementation of the novel hybrid MLP-FFA method for prediction of biochemical oxygen demand and dissolved oxygen: a case study of Langat River. Environ Earth Sci. https://doi.org/10.1007/s12665-017-6842-z
- Ren T, Liu X, Niu J, Lei X, Zhang Z (2020) Real-time water level prediction of cascaded channels based on multilayer perception and recurrent neural network. J Hydrol 585:124783. https://doi.org/10.1016/j.jhydrol.2020. 124783
- Rummel R, Sjöberg LE, Rapp R (1978) The determination of gravity anomalies from geoid heights using the inverse Stokes' formula, Fourier transforms, and least squares collocation. NASA Contract Report 141442, Department of Geodetic Science, The Ohio State University, Columbus, Ohio, USA. pp 65
- Schwingshackl D, Rehrl J, Horn M, Belz J, Nelles O (2017) Model extension for model-based MIMO control in HVAC systems. J Build Eng 11:224–229. https://doi.org/10.1016/j.jobe.2017.04.015
- Shoorehdeli MA, Teshnehlab M, Sedigh AK (2007) Novel Hybrid Learning Algorithms for Tuning ANFIS Parameters Using Adaptive Weighted PSO. In: 2007 IEEE International Fuzzy Systems Conference. https://doi.org/10.1109/fuzzy.2007.4295571
- Smith WHF, Moose RE (1997) Comparison of marine gravity anomalies measured by ships and estimated from satellite altimetry in near-shore areas, Eos Trans. AGU, Spring Meet. Suppl., S103.
- Smith WHF, Sandwell DT, Raney RK (2005) Bathymetry from satellite altimetry: Present and future. Proceedings of OCEANS 2005 MTS/IEEE, IEEE, Washington, DC, USA. pp 2586–2589, https://doi.org/10.1109/OCEANS.2005. 1640160
- Soltanpour A, Pirooznia M, Aminjafari S, Zareian P (2017) Persian Gulf and Oman Sea tide modeling using satellite altimetry and tide gaugedata (TM-IR01). Mar Georesour Geotechnol. https://doi.org/10.1080/1064119x. 2017.1366608
- Suparta W, Alhasa KM (2013) A comparison of ANFIS and MLP models for the prediction of precipitable water vapor. In: 2013 IEEE International Conference on Space Science and Communication (IconSpace), vol. 29. pp 243–248. https://doi.org/10.1109/iconspace.2013.6599473

- Teja G, Rao MN (2011) Image retrieval system using fuzzy-softmax MLP neural network. Indian J Appl Res 3(6):169–174. https://doi.org/10.15373/22495
- Tenzer R, Chen W, Jin SG (2015) Effect of the upper mantle density structure on the Moho geometry. Pure Appl Geophys 172(6):1563–1583. https://doi.org/10.1007/s00024-014-0960-2
- Teruzzi A, Dobricic S, Solidoro C, Cossarini G (2014) A 3-D variational assimilation scheme in coupled transport-biogeochemical models: forecast of Mediterranean biogeochemical properties. J Geophys Res Oceans 119(1):200–217. https://doi.org/10.1002/2013JC009277
- Than NH, Ly CD, Van Tat P (2021) The performance of classification and forecasting Dong Nai River water quality for sustainable water resources management using neural network techniques. J Hydrol 596:126099. https://doi.org/10.1016/j.jhydrol.2021.126099
- Thompson AF, Richards KJ (2011) Low frequency variability of Southern Ocean jets. J Geophys Res. https://doi.org/10.1029/2010JC006749
- Volpe G, Colella S, Brando VE, Forneris V, La Padula F, Di Cicco A, Sammartino M, Bracaglia M, Artuso M, Santoleri R (2019) Mediterranean Ocean colour level 3 operational multi-sensor processing. Ocean Sci 15(1):127–146. https://doi.org/10.5194/os-15-127-2019
- Vrdoljak L, Bašić T (2023) Bathymetry estimation from satellite altimeterderived gravity data. Satell Altim the Appl Recent Adv. https://doi.org/10. 5772/intechopen.108511
- Wan X, Ran J, Jin S (2019) Sensitivity analysis of gravity anomalies and vertical gravity gradient data for bathymetry inversion. Mar Geophys Res 40:87–96. https://doi.org/10.1007/s11001-018-9361-8
- Watts AB (1978) An analysis of isostasy in the World's Oceans. 1- Hawaiian-Emperor Seamount Chain. J Geophys Res 83:5985–6004
- Wiehle S, Martinez B, Hartmann K, Verlaan M, Thornton T, Lewis S, Schaap D (2016) the BASE-platform project: deriving the bathymetry from combined satellite data. www.base-platform.com
- Wollheim WM, Harms TK, Robison AL, Koenig LE, Helton AM, Song C, Bowden WB, Finlay JC (2022) Superlinear scaling of riverine biogeochemical function with watershed size. Nat Commun 13(1):1–9. https://doi.org/10.1038/s41467-022-28630-z
- Xu C, Li J, Jian G, Wu Y, Zhang Y (2023) An adaptive nonlinear iterative method for predicting seafloor topography from altimetry-derived gravity data. J Geophys Res Solid Earth. https://doi.org/10.1029/2022JB025692
- Yang S, Yang D, Chen J, Zhao B (2019) Real-time reservoir operation using recurrent neural networks and inflow forecast from a distributed hydrological model. J Hydrol 579:124229. https://doi.org/10.1016/j.jhydrol.2019.
- Yonkee WA, Weil AB (2015) Tectonic evolution of the Sevier and Laramide belts within the North American Cordillera orogenic system. Earth-Sci Rev 150:531–593. https://doi.org/10.1016/j.earscirev.2015.08.001
- Yuan Z, Chen H, Wang Y, Li X (2025) Seabed depth prediction using multi-scale gravity anomalies and fully connected deep neural networks: a novel approach applied to the South China Sea. Remote Sens 17(3):412. https://doi.org/10.3390/rs17030412
- Zhang D, Lindholm G, Ratnaweera H (2018) Use long short-term memory to enhance Internet of Things for combined sewer overflow monitoring. J Hydrol 556:409–418. https://doi.org/10.1016/j.jhydrol.2017.11.018
- Zhang YY, Wang ZH, Zou ZJ (2022) Black-box modeling of ship maneuvering motion based on multi-output nu-support vector regression with random excitation signal. Ocean Eng 257:111279. https://doi.org/10.1016/j.oceaneng.2022.111279
- Zhou S, Li X, Sun Y, Chang X, Jia Y, Guo J, Sun H (2024) Predicting bathymetry using multisource differential marine geodetic data with multilayer perceptron neural network. Earth Syst Sci Data 17(1):165–179. https://doi.org/10.5194/essd-17-165-2025
- Zhou S, Guo J, Zhang H, Jia Y, Sun H, Liu X, An D (2025) SDUST2023BCO: A global seafloor model determined from a multi-layer perceptron neural network using multi-source differential marine geodetic data. Earth Syst Sci Data 17(1):165–179. https://doi.org/10.5194/essd-17-165-2025

Mohammad et al. Geoscience Letters (2025) 12:53 Page 18 of 18

- Zhu Q, Wiberg PL (2022) The importance of storm surge for sediment delivery to microtidal marshes. J Geophys Res Earth Surf 127(9):e2022JF006612. https://doi.org/10.1029/2022JF006612
- Zingerle P, Pail R, Gruber T et al (2020) The combined global gravity field model XGM2019e. J Geod 94:66. https://doi.org/10.1007/s00190-020-01398-0
- Zounemat-Kermani M, Matta E, Cominola A, Xia X, Zhang Q, Liang Q, Hinkelmann R (2020) Neurocomputing in surface water hydrology and hydraulics: a review of two decades retrospective, current status and future prospects. J Hydrol 588:125085. https://doi.org/10.1016/j.jhydrol. 2020.125085

# **Publisher's Note**

Springer Nature remains neutral with regard to jurisdictional claims in published maps and institutional affiliations.